Available online at www.sciencedirect.com
ScienceDirect
Journal of Environmental Sciences 2011, 23(2) 236–246
JOURNAL OF ENVIRONMENTAL SCIENCES
ISSN 1001-0742
CN 11-2629/X
www.jesc.ac.cn

A numerical study of summer ozone concentration over the Kanto area of Japan using the MM5/CMAQ model

Mai Khiem[1,*], Ryozo Ooka[2], Hong Huang[3], Hiroshi Hayami[4]

1. Graduate School of Engineering, The University of Tokyo, 4–6–1 Komaba, Meguro-ku, Tokyo 153–8505, Japan. E-mail: khiem@iis.u-tokyo.ac.jp
2. Institute of Industrial Science, The University of Tokyo, 4–6–1 Komaba, Meguro-ku, Tokyo 153–8505, Japan
3. Center for Public Safety Research, Tsinghua University, Beijing 100084, China
4. Central Research Institute of Electric Power Industry, 1646 Abiko, Abiko-shi, Chiba 270–1194, Japan

Received 10 February 2010; revised 06 July 2010; accepted 21 September 2010

Abstract

We assessed the ability of the MM5/CMAQ model to predict ozone (O_3) air quality over the Kanto area and to investigate the factors that affect simulation of O_3. We find that the coupled MM5/CMAQ model is a useful tool for the analysis of urban environmental problems. The simulation results were compared with observational data and were found to accurately replicate most of the important observed characteristics. The initial and boundary conditions were found to have a significant effect on simulated O_3 concentrations. The results show that on hot and dry days with high O_3 concentration, the CMAQ model provides a poor simulation of O_3 maxima when using initial and boundary conditions derived from the CMAQ default data. The simulation of peak O_3 concentrations is improved with the JCAP initial and boundary conditions. On mild days, the default CMAQ initial and boundary conditions provide a more realistic simulation. Meteorological conditions also have a strong impact on the simulated distribution and accumulation of O_3 concentrations in this area. Low O_3 concentrations are simulated during mild weather conditions, and high concentrations are predicted during hot and dry weather. By investigating the effects of different meteorological conditions on each model process, we find that advection and diffusion differ the most between the two meteorological regimes. Thus, differences in the winds that govern the transport of O_3 and its precursors are likely the most important meteorological drivers of ozone concentration over the central Kanto area.

Key words: air quality modeling; ozone; initial/boundary conditions; meteorological conditions

DOI: 10.1016/S1001-0742(10)60398-1

Citation: Khiem M, Ooka R, Huang H, Hayami H, 2011. A numerical study of summer ozone concentration over the Kanto area of Japan using the MM5/CMAQ model. Journal of Environmental Sciences, 23(2): 236–246

Introduction

For decades, ground-level ozone has been recognized as a harmful pollutant because it is the primary ingredient in photochemical smog and has detrimental effects on human health and the environment (Lippmann, 1991). The formation of ozone has been well documented. A secondary air pollutant, ozone is produced by a series of complex chemical reactions, and its overall concentration is influenced by a variety of physical processes including advection, diffusion, and deposition. Understanding the relationships between these processes and identifying which processes are dominant cannot be achieved by observation analysis alone due to the limited number of available measurements. Numerical simulations use assumed physical and chemical processes to link emissions and ambient concentrations, thus providing a powerful tool for the analysis of ozone formation.

Over the past several decades, extensive modeling studies have been conducted to quantify air pollution drivers and impacts. Early studies used the Urban Airshed Model (UAM) (Morris and Meyers, 1990) and the Regional Oxidant Model (ROM) (Lamb, 1983a, 1983b). More recently, a third-generation air quality model, known as the Community Multiscale Air Quality (CMAQ) model, has become a powerful tool for applications ranging from regulatory to research studies (Byun and Ching, 1999) and is now very popular. The CMAQ model is a multi-pollutant, multi-scale air quality modeling system that uses state-of-science techniques to simulate all atmospheric and land processes that affect the transport, transformation and deposition of atmospheric pollutants and/or their precursors on both regional and urban scales (Byun and Ching, 1999). For simulation of meteorological fields, the state-of-the-art atmospheric dynamic simulator MM5 (fifth-generation Penn State/NCAR Mesoscale Model) has been integrated with CMAQ in many air quality studies. Zhang et al. (2006) presented a comprehensive performance evaluation of the MM5-CMAQ system in the southern United States. Sokhi et al. (2006) predicted ozone levels in London using the MM5-CMAQ modeling system. Chen et al. (2007) used

* Corresponding author. E-mail: khiem@iis.u-tokyo.ac.jp

the MM5-CMAQ model to investigate PM_{10} air pollution in Beijing, China.

Over the last few decades, a number of studies have simulated the temporal and spatial distribution of ozone and other pollutants over the Kanto area (Fig. 1) (e.g., Kimura, 1985; Ohara et al., 1997; Uno et al., 2005). These studies showed that the transport of air pollutants has a substantial impact on ozone distribution and that numerical simulations are useful for analysis of photochemical air pollution in this area. For example, Kimura (1985) examined the basic characteristics of air pollution in the Kanto area using a model of local winds coupled with a simplified chemical reaction model. His results helped explain the transport of photochemical air pollutants to the area. He found that summertime ozone episodes in the rural inland portion of the region occur following horizontal transport associated with the inland penetration of the sea breeze and its interaction with both mountain-valley winds and synoptic winds. Ohara et al. (1997) developed a three-dimensional air pollution model to simulate regional-scale photochemical oxidant episodes in the summer and applied it to the Kanto area. Their results were compared with observational data and showed reasonable agreement. Uno et al. (2005) developed the RAMS/CMAQ Asia-scale chemical transport modeling system to be applied to Asia and Japan. However, few studies have used numerical models to analyze the factors that affect photochemical air pollution. Application of the MM5/CMAQ air quality model to the Kanto area has been limited, and a detailed evaluation of the system in this region has not been performed. Comparisons against observations provide valuable information about model performance.

Initial and boundary conditions are required for performing model simulations and play an important role in simulating regional air quality (Berge et al., 2001; Liu et al., 2001; Jimenez et al., 2007). Initial conditions are specified within the simulation domain at the beginning of the simulation, while boundary conditions are prescribed throughout the simulation period. The CMAQ model currently uses a static profile of clean air as the chemical initial and boundary conditions for air quality simulations. The assumption of clean air conditions may be not suitable for simulations on highly polluted days. It is extremely important to evaluate the influence of the choice of initial and boundary conditions and to obtain appropriate values for regional-scale simulations (Liu et al., 2001).

The purpose of this article is to assess the ability of the MM5/CMAQ model to predict ozone air quality over the Kanto area and to investigate the factors that affect the simulation of ozone concentrations. We first use the MM5/CMAQ model to simulate ozone levels during two periods in the summer and evaluate the performance of the model in the Kanto area. We then investigate the influence of initial and boundary conditions on the ozone simulation. We also use the model simulation to examine the impact of meteorological conditions on the distribution of ozone concentrations.

1 Model description and numerical experiments

1.1 Models

The MM5 model (version 3.7) is a limited-area, non-hydrostatic, terrain-following sigma-coordinate model (Dudhia et al., 2005). MM5 was used in this study to provide the spatial and temporal distributions of the meteorological fields required by the air quality model. The CMAQ model (version 4.6), developed by the U. S. Environmental Protection Agency and released in 2006, was also used in this study. CMAQ is a multi-scale and multiple-pollutant chemical transport model that includes the following processes: atmospheric transport, deposition, cloud mixing, emissions, gas- and aqueous-phase chemical transformation, and aerosol dynamics and chemistry. The meteorological input data for CMAQ are generated by the MM5 model. The one-way "offline" coupling of

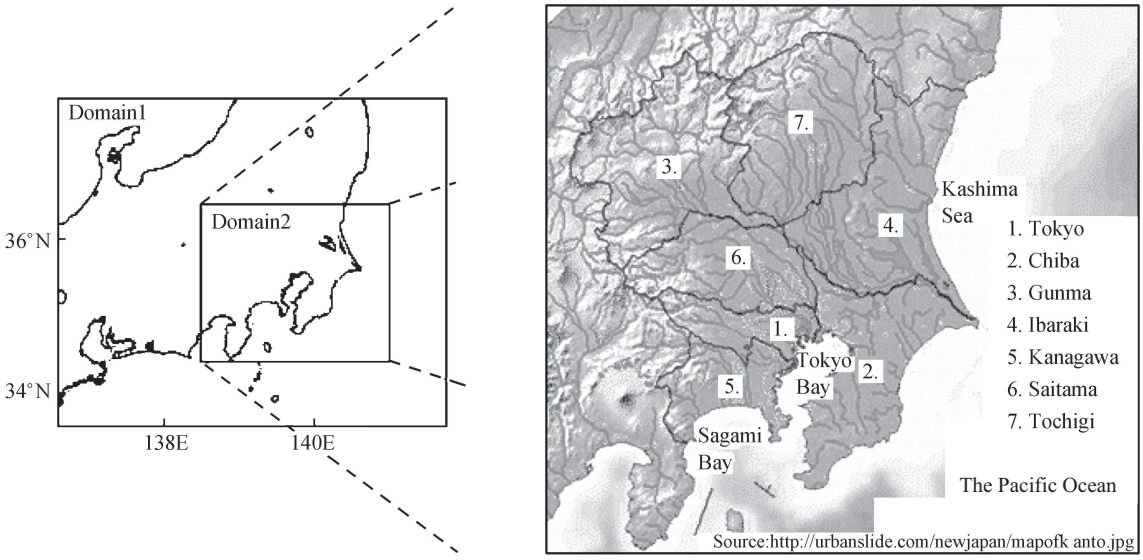

Fig. 1 Analysis domain for the MM5/CMAQ model simulations.

MM5 to CMAQ is accomplished through a meteorology–chemistry interface processor (MCIP) that handles window domain mapping, data format translation, unit conversion, diagnostic estimates of derived variables, and reconstructions of meteorological inputs on different horizontal and vertical grids through simple bilinear interpolation (Byun and Ching, 1999). We also used the Integrated Process Rate (IPR) analysis tool available in CMAQ to conduct a detailed process analysis of ozone formation. The change in the concentration of a given chemical species caused by various physical and chemical processes can be described using the mass conservation equations as follows:

$$\frac{\partial C_i}{\partial t} = -\left[\frac{\partial}{\partial x}(uC_i) + \frac{\partial}{\partial y}(vC_i) + \frac{\partial}{\partial z}(wC_i)\right]_{ADV} + \left[\frac{\partial}{\partial x}\left(K_x\frac{\partial C_i}{\partial x}\right) + \frac{\partial}{\partial y}\left(K_y\frac{\partial C_i}{\partial y}\right) + \frac{\partial}{\partial z}\left(K_z\frac{\partial C_i}{\partial z}\right)\right]_{DIF} + CHEM_i + EMIS_i + \left(\frac{\partial C_i}{\partial t}\right)_{DDEP} + \left(\frac{\partial C_i}{\partial t}\right)_{WDEP} + \left(\frac{\partial C_i}{\partial t}\right)_{Cloud} + \left(\frac{\partial C_i}{\partial t}\right)_{Aerosols} \quad (1)$$

where, C_i is the concentration of the species of interest; u, v,and w are the components of the velocity vector at each grid point within the model domain; K is the eddy diffusivity used to parameterize the subscale turbulent fluxes of the species; ADV is advection; DIF is diffusion; CHEM is the net rate of chemical transformation (production and loss); EMIS is the emission rate; and DDEP, WDEP, CLOUD, and AEROSOLS are the rates of change of concentration due to dry deposition, wet deposition, clouds, and aerosols, respectively (Byun and Ching, 1999).

1.2 Outline and set-up of the numerical experiments

The MM5 simulation was performed within two nested domains (Fig. 1). A detailed configuration of the model is summarized in Table 1. The two domains cover the Kanto region with grid resolutions of 9 and 3 km, respectively. Only the 3-km resolution MM5 output was used to drive the air quality model. Both domains have 23 vertical sigma levels from the surface to 100 hPa. The σ coordinate of the lowest model layer is at 0.998, which is equivalent to about 14 m above the ground.

Table 1 Analysis domain sizes and grid resolution

Domain	Computation domain (X (km) × Y (km))	Number of grid cells ($nx_x ny_x nz$)	Horizontal resolution (km)
D1	450 × 540	51 × 61 × 23	9
D2	216 × 261	73 × 88 × 23	3

The physical configuration used in the MM5 simulation is as follows: the Grell et al. (1994) cumulus parameterization scheme; the MRF planetary boundary layer scheme (Hong et al., 1996); explicit simple ice microphysics (Hsie et al., 1984); the cloud-radiation scheme (Dudhia, 1989) and Four-dimensional data assimilation (FDDA). The cumulus parameterization scheme was not used in the 3-km domain. CMAQ was configured with the following options: (1) CB-IV speciation with aerosol and aqueous chemistry; (2) the Piecewise Parabolic Method for both horizontal and vertical advection; (3) eddy vertical diffusion; (4) photolysis; (5) no Plume-in-Grid; (6) the EBI chemistry solver configured for CB-IV; (7) the 3rd-generation aerosol model; (8) the 2nd-generation aerosol deposition model; and (9) the RADM cloud model. A more detailed description of the scientific mechanisms implemented in CMAQ can be found in Byun and Ching (1999). To decrease the computation time and reduce the size of output files, the 23-layer output from MM5 was transformed into 14 layers for input into CMAQ using the MCIP program. The layers are most closely spaced near the surface, and the lowest layer extends from the surface to about 14 m above the ground.

Two analysis periods were selected for MM5/CMAQ simulation: (1) from 09:00 JST July 19 to 09:00 JST July 23, 2005 and (2) from 09:00 JST August 3 to 09:00 JST August 7, 2005. These periods were chosen because they reflect typical summer weather patterns. High solar radiation was recorded during both periods, as shown in Fig. 2a and b. Both simulations included a 15-hour "spin up" period for cloud processes that was not used for the CMAQ simulation. Final analysis data (FNL) from the National Centers for Environmental Prediction (NCEP) with horizontal resolution of 1° ×1° and temporal resolution of six hours were used to provide the initial and boundary conditions for the MM5 model and the FDDA process. The terrain, land use and land water mask datasets were obtained from the United States Geological Survey (USGS). The USGS 25-category land use/land cover classification was used to determine the single dominant land use type for each computation cell. Hourly emissions estimates

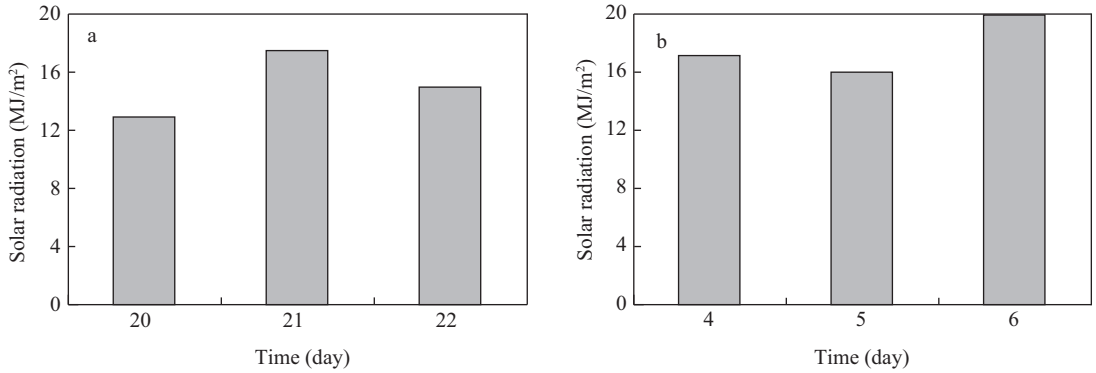

Fig. 2 Total solar radiation during 8:00–15:00 JST in Tokyo for (a) July 20–21 and (b) August 4–6. Data were collected from Tokyo meteorological stations.

from Hayami and Kobayashi (2004) were used for NOx and non-methane hydrocarbons (NMHC), which included paraffin carbon bond (PAR), ethane (ETH), olefin (OLE), toluene (TOL), xylene (XYL), formaldehyde (FORM), aldehydes (ALD), and isoprene (ISO). Figure 3 shows an example of the emission data on the 3-km grid at 14:00 JST. Emissions included area sources, point sources, mobile sources and biogenic sources. After completing the MM5 simulation, the CMAQ model was run in the 3-km domain for two periods: from 00:00 JST on July 20 to 00:00 JST on July 23 and from 00:00 JST on August 4 to 00:00 JST on August 7.

Two case studies were conducted to assess the influence of the initial and boundary conditions. Case 1 used the Japan Clean Air Program data (JCAP, 1999), which were obtained by extrapolating data from air quality monitoring sites across the Kanto area. Case 2 used the CMAQ default values, which were derived from climatological profiles of atmospheric pollutants (clean air) as described in Byun and Ching (1999). The initial and boundary conditions for these cases are summarized in Table 2. The initial and boundary ozone concentrations were almost the same for the two case studies. NOx and NMHC concentrations were higher for Case 1 than Case 2, which was characterized by cleaner air.

1.3 Evaluation measures

General guidance and protocols for evaluating air quality model performance have been provided by the US EPA (2006). The statistical measures include the mean bias (MB), the root mean squared error (RMSE), the mean normalized bias error (MNBE), the mean normalized gross error (MNGE), the mean fractional bias (FBIAS), the mean error (ME), the mean fractional error (FERROR) and correlation coefficients (CC), which are calculated for hourly ozone and 8-hourly maximum ozone over the days spanning a pollution episode. In this study, the simulation results were evaluated statistically using the following measures:

$$\mathrm{MB} = \frac{1}{N}\sum_{i=1}^{N}(M_i - O_i) \tag{2}$$

$$\mathrm{ME} = \frac{1}{N}\sum_{i=1}^{N}|M_i - O_i| \tag{3}$$

$$\mathrm{RMSE} = \sqrt{\frac{1}{N}\sum_{i=1}^{N}(M_i - O_i)^2} \tag{4}$$

$$\mathrm{CC} = \frac{\sum_{i=1}^{N}(M_i - \overline{M_i})(O_i - \overline{O_i})}{\sqrt{\sum_{i=1}^{N}(M_i - \overline{M_i})^2}\sqrt{\sum_{i=1}^{N}(O_i - \overline{O_i})^2}} \tag{5}$$

$$\mathrm{MNBE} = \frac{1}{N}\sum_{i=1}^{N}\left(\frac{M_i - O_i}{O_i}\right) \times 100\% \tag{6}$$

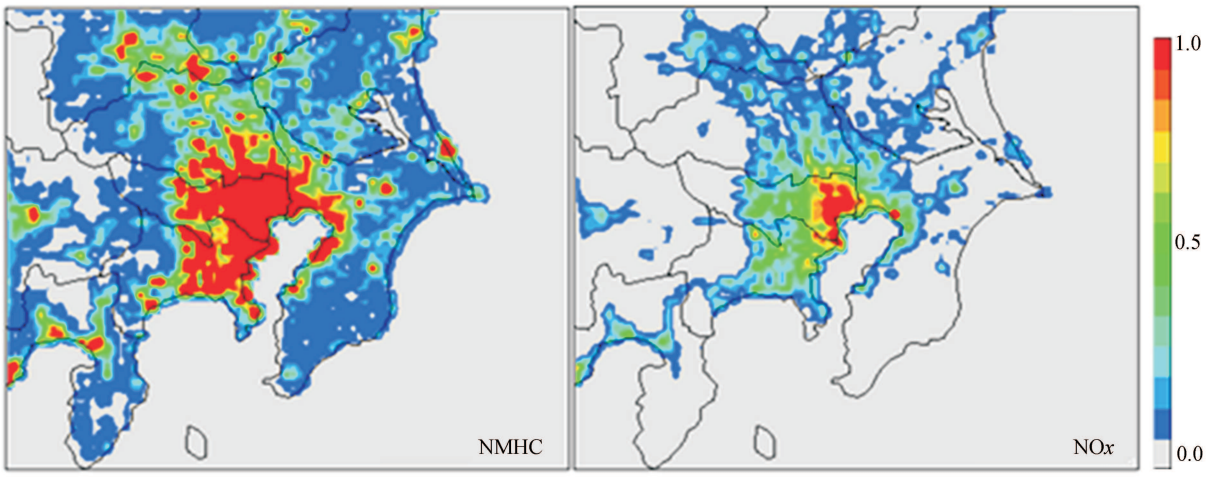

Fig. 3 Hourly emission data used in the CMAQ model at 14:00 JST (mole/sec grid).

Table 2 Description of the chemical initial and boundary conditions in the first layer (14 m) and top layer (12,000 m) of the CMAQ simulations

Case	Initial condition (IC) & boundary condition (BC)		O_3 (ppb)		NOx (ppb)		NMHC (ppb)	
			First layer	Top layer	First layer	Top layer	First layer	Top layer
Case 1[a]	IC		28.00	70.00	6.00	0.00	98.90	0.71
	BC	North	28.00	70.00	6.00	0.00	98.90	0.71
		East	25.00	70.00	6.00	0.00	98.90	2.18
		South	30.00	70.00	6.00	0.00	51.70	0.35
		West	28.00	70.00	6.00	0.00	130.50	0.30
Case 2[b]	IC		35.00	70.00	0.25	0.00	2.74	0.71
	BC	North	35.00	70.00	0.25	0.00	2.74	0.71
		East	30.00	70.00	0.01	0.00	2.42	2.18
		South	30.00	70.00	0.02	0.00	2.42	0.35
		West	35.00	70.00	0.25	0.00	3.42	0.30

[a] Case 1 used the Japan Clean Air Program data (JCAP, 1999); [b] case 2 used the CMAQ default values.

$$\mathrm{MNGE} = \frac{1}{N}\sum_{i=1}^{N}\left|\frac{M_i - O_i}{O_i}\right| \times 100\% \quad (7)$$

where, M_i is the hourly-averaged model-predicted concentration in the grid cell corresponding to the location of a monitoring site, O_i is the observed concentration at that site for the same hour, the index i represents a valid simulation-observation pair, and N is the total number of valid pairs.

2 Results and discussion

2.1 Evaluation of MM5 model performance

To evaluate the MM5 model simulation, wind speed and direction at 10-m altitude and temperature at 2-m altitude were compared to the observed data from July 20 to 22 and August 4 to 6, 2005 at four sites across the Kanto area: Nerima, Ebina, Saitama, and Abiko (Fig. 4). Here the simulated 2-m temperature and 10-m winds were estimated from the lowest sigma level using the Monin-Obukhov similarity theory. The MM5 performance statistics at the four sites are summarized in Table 3 for July 20 to 22 and for August 4 to 6. The wind speed exhibits positive biases at all sites except Saitama. The MB and ME of the wind speed are 0.4 to 1.3 m/sec and 1.2 to 1.6 m/sec, respectively, for July 20 to 22. For August 4 to 6, the MB and ME are –0.1 to 1.0 m/sec and 0.8 to 1.1 m/sec, respectively. The MM5 wind direction biases are generally large, with the ME reaching approximately 110° at the Saitama site in August. The temperature biases are positive at all sites in both periods. The MB and ME of the temperature show larger biases in July than in August. The magnitude of the RMSE and CC are used to determine the accuracy of the simulation. The RMSE of temperature at all sites is 1.8 to 2.7°C in July and 1.9 to 2.5°C in August. The CC of the temperatures is high, especially from August 4 to 6 when it is more than 0.9 at all sites. These results suggest that more accurate temperatures are simulated during the hot episode than during milder weather. The RMSE and CC are not as good for the wind speeds and directions as for temperature. Nonetheless, these values indicate that the MM5 meteorological simulations are reasonably accurate and can be used to simulate ozone concentrations over the Kanto area.

Fig. 4 Monitoring stations used for the MM5/CMAQ model validation.

2.2 Ozone simulation and the influence of initial and boundary conditions

Results from the CMAQ model were compared with observational data from the four air quality monitoring sites shown in Fig. 4. Figures 5 and 6 show the observed and simulated variation of hourly-averaged O_3 for the two cases. Modeled concentrations are taken from the lowest level of the CMAQ model. Generally, ozone concentrations were higher at all sites during August 4 to 6 than during July 20 to 22. The observed peak ozone concentrations were approximately 40 to 90 ppb in July and 60 to 150 ppb in August, while the nighttime minima fell to nearly zero during both periods. CMAQ provides a fairly accurate simulation of the diurnal ozone variation, although differences in magnitude are seen between the cases, especially for the simulated peak ozone concentration.

During July 20 to 22, model over-predictions are found at all sites in Case 1. The simulated peak concentrations at these sites are approximately 84 to 105 ppb. Larger deviations are found for sites with lower observed O_3 concentrations, such as Ebina. In Case 2, when the CMAQ default data are used for the initial and boundary conditions, the CMAQ model accurately reproduces the observed O_3 concentrations at all sites.

During August 4 to 6, the simulated magnitudes in Case 1 agree reasonably well with the observed concen-

Table 3 Summary of MM5 performance statistics for July 20 to 22 and August 4 to 6

Site	Wind speed (m/sec)				Wind direction (deg.)				Temperature (°C)			
	MB	ME	RMSE	CC	MB	ME	RMSE	CC	MB	ME	RMSE	CC
July 20 to 22												
Nerima	1.3	1.4	1.6	0.3	-30.4	45.2	59.5	0.7	1.8	2.1	2.5	0.9
Ebina	1.2	1.5	1.8	0.3	-11.4	57.5	109.6	0.3	1.3	1.5	1.8	0.9
Saitama	0.4	1.2	1.4	0.4	24.0	66.6	103.8	0.4	2.4	2.4	2.7	0.9
Abiko	1.3	1.6	1.9	0.4	-4.2	34.7	58.8	0.7	2.1	2.2	2.6	0.9
August 4 to 6												
Nerima	0.8	0.9	1.0	0.6	–6.0	35.6	56.2	0.6	1.6	1.7	1.9	0.9
Ebina	0.5	0.9	1.1	0.7	–4.6	51.5	77.3	0.2	1.5	1.6	1.9	0.9
Saitama	–0.1	0.8	0.9	0.4	74.7	110.0	145.7	0.0	1.7	1.7	2.0	1.0
Abiko	1.0	1.1	1.3	0.8	25.5	32.2	44.2	0.8	2.3	2.3	2.5	1.0

MB: mean bias; ME: mean error; RMSE: root mean squared error; CC: correlation coefficient.

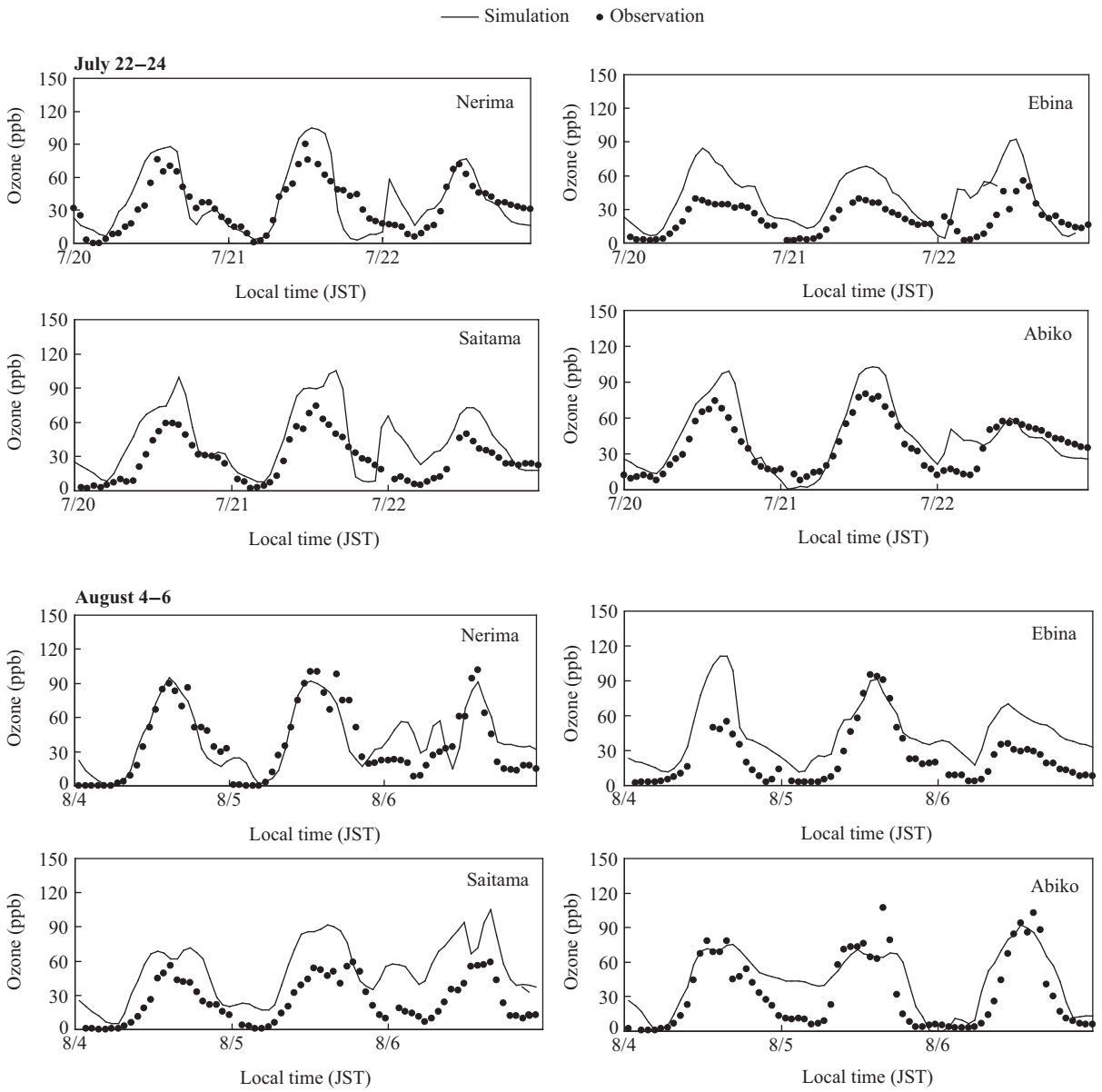

Fig. 5 Time series of observed and simulated ozone concentrations at the four sites for Case 1 during July 20 to 22 and August 4 to 6.

trations, although there is a tendency for over-prediction at night for all sites and during the day at sites with low observed O_3 concentrations (e.g., Ebina and Saitama). The higher simulated O_3 concentrations at night may be related to the calculation of the vertical diffusion coefficient in MM5, the emission data, or the chemistry. Using the CMAQ default data, the CMAQ model does not accurately simulate the peak O_3 concentrations except at Saitama. The simulated peak concentrations at these sites in Cases 1 and 2 are approximately 91 to 112 and 37 to 76 ppb, respectively, compared to r observed peaks of 60 to 150 ppb.

Performance statistics for the CMAQ simulation are summarized in Table 4 for July 20 to 22 and for August 4

Table 4 Summary of CMAQ performance statistics for O_3 concentration (ppb) for July 20 to 22 and August 4 to 6

Monitoring site	Case 1				Case 2			
	MB	ME	RMSE	CC	MB	ME	RMSE	CC
July 20 to 22								
Nerima	4.4	14.7	18.4	0.8	–11.6	17.0	20.9	0.6
Ebina	20.1	21.4	25.1	0.8	4.8	10.3	12.1	0.6
Saitama	17.0	19.6	23.4	0.8	2.0	11.7	14.5	0.7
Abiko	7.8	12.6	15.6	0.9	–8.6	13.8	15.3	0.8
August 4 to 6								
Nerima	4.7	13.8	17.0	0.9	–18.9	22.0	30.0	0.7
Ebina	21.2	22.0	25.4	0.8	2.0	13.6	18.8	0.6
Saitama	26.9	27.3	30.7	0.8	2.1	12.1	15.0	0.7
Abiko	11.4	15.5	19.9	0.9	–6.0	15.3	20.6	0.8

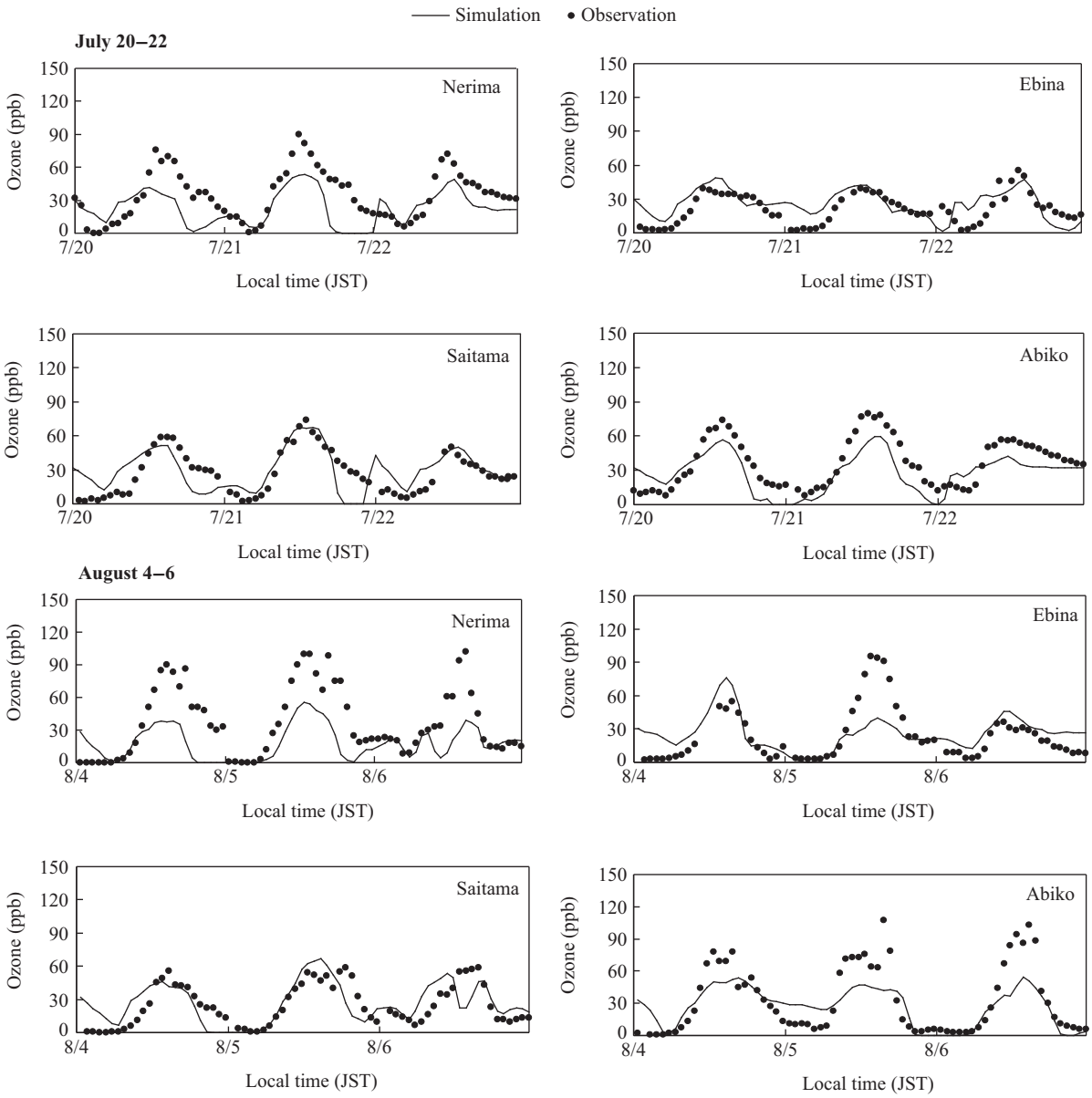

Fig. 6 Time series of observed and simulated ozone concentrations at the four sites for Case 2 during July 20 to 22 and August 4 to 6.

to 6. Overall, the CC values are high for both periods, with a maximum of 0.9 in Case 1. The O_3 concentration RMSE ranges from 11.5 to 30.7 ppb, indicating that the CMAQ model can reproduce surface O_3 concentrations reasonably well. The MB and ME values show that the O_3 biases in Case 1 are positive at all sites during both periods. The positive bias in July is attributed to over-prediction of O_3 during both night and day, while in August it is attributed to over-prediction of O_3 at night. For Case 2, smaller biases in July are found at all sites, as shown in Table 5. However, due to the hotter conditions in August, negative biases are found at Nerima and Saitama. Table 5 shows the MNBE and MNGE for episodes with surface ozone concentrations of 40 ppb or higher (pairs of simulated and observed O_3 were excluded when the observed value was $\leqslant$ 40 ppb). For each case, the values of MNBE and MNGE were within the limits suggested by US EPA (2006) for urban-scale modeling (MNBE $\leqslant \pm$15%, MNGE $\leqslant$ 35%), except for Case 1 during July 20 to 22 and Case 2 during August 4 to 6, when the MNBE was slightly higher than the EPA-recommended value. These results suggest that the simulated results are reasonably accurate and can be used to analyze ozone formation over the Kanto area.

Table 5 Statistical metrics for surface ozone with concentration greater than 40 ppb

Episode		Case 1	Case 2
July 20–22	MNBE	23.2	–29.0
	MNGE	35.9	30.8
August 4–6	MNBE	19.7	–34.5
	MNGE	32.3	42.7

Comparison of the two case studies shows that the initial and boundary conditions have a significant impact on the simulation of O_3. During the milder episode (July), the peak O_3 concentrations simulated in Case 1 are too high relative to the observations at all sites except Nerima. The RMSE (15.6 to 25.6 in Case 1 and 10.7 to 20.9 in Case 2) suggests that the CMAQ default data provide a more

accurate simulation than the JCAP data (1999). In contrast, during the hotter August episode (generally associated with high O_3 concentrations), the CMAQ simulations in Case 2 do not match the observed peak O_3 concentrations, which exceed the Environmental Quality Standards (one-hour value of 0.06 ppm or less). The observed O_3 maxima are reasonably well reproduced by the simulation with initial and boundary conditions from JCAP (1999).

To better understand the simulated ozone maxima in hot and dry weather conditions, IPR was used to assess and quantify the contributions of the different physical and chemical processes to ozone simulated on August 6. Table 6 summarizes the total change in ozone concentration in the first model level between 08:00 and 15:00 JST caused by four major processes: advection (ADV, horizontal and vertical components), diffusion (DIF, mostly dominated by its vertical component), dry deposition (DDEP), and chemistry (CHEM). This 8-hr period is representative of the timescale over which ozone concentrations increase in the Kanto region; it also determines whether and to what degree ozone air quality standards are exceeded. The hourly-averaged ozone rates of change due to each process show that ground-level ozone concentrations are primarily enhanced by diffusive influx of ozone from aloft, whereas chemistry, advection and dry deposition mainly deplete ozone. The CHEM term is negative close to ground, probably due to ozone titration by NO*x*. Ozone is produced photochemically at higher levels in the atmosphere, as shown in Table 7. This ozone from aloft is then mixed down toward the surface. Tables 6 and 7 show that more high-altitude chemical ozone production occurs in Case 1 than in Case 2, leading to a significant increase in the diffusion term in Case 1 (given the same meteorological conditions). As a result, the deposition and advection terms are larger in Case 1. There is also less chemical ozone destruction (CHEM) in the surface layer in Case 1 at all sites but Nerima, which is located near a major emission source. These differences may be due to the enhanced concentrations of ozone precursors in Case 1, as shown in Table 8.

The high concentrations of NMHC that characterize Case 1 provide a source of NO_2, which is necessary to start the ozone formation cycle in an NMHC-limited urban atmosphere (Kannari, 2006):

$$RO_2 + NO \longrightarrow NO_2 + HO_2 + \text{other products} \quad (8)$$

$$HO_2 + NO \longrightarrow NO_2 + OH \quad (9)$$

Reactions (8) and (9) represent simplifications of a series of complex chemical reactions in which hydroperoxy radicals (HO_2) and organic peroxy radicals (RO_2) are produced through photochemical oxidation of NMHC. When more NMHC molecules are added to the atmosphere, a greater proportion of NO is oxidized to NO_2 by peroxy radicals (RO_2 and HO_2). These newly-produced NO_2 molecules undergo photolysis, producing oxygen atoms ($O(^3P)$) and thus O_3 via reaction of $O(^3P)$ with O_2.

The reduced NMHC concentrations in Case 2 lead to a significant decrease in photochemical ozone production relative to Case 1 (Tables 7 and 8). As a result, the simulation in Case 2 does not reproduce the observed peak O_3 concentrations on August 6.

Table 6 Summary of the total change in ozone concentration (ppb/8 hr) due to different processes in the first model level between 08:00 and 15:00 JST on August 6

Case	Process	Nerima	Ebina	Saitama	Abiko
Case 1	ADV	–59.5	–92.1	–34.1	–9.2
	CHEM	–295.2	–137.5	–15.5	25.2
	DIF	514.4	645.5	500.5	483.1
	DDEP	–133.5	–408.8	–415.8	–469.2
Case 2	ADV	–19.1	–66.0	–35.3	–36.6
	CHEM	–287.2	–187.8	–46.9	–53.8
	DIF	372.9	519.2	296.8	353.2
	DDEP	–57.8	–260.2	–217.1	–237.4

ADV: advection; CHEM: chemistry; DIF: diffusion; DDEP: dry deposition.

Table 7 Total change in ozone concentration (ppb/8 hr) due to the CHEM process in the third and fifth model levels (about 135 and 462 m above the ground) between 08:00 and 15:00 JST on August 6

Layer	Case	Nerima	Ebina	Saitama	Abiko
Layer 3	Case 1	9.9	57.1	51.6	89.9
	Case 2	–36.6	31.7	23.4	32.6
Layer 5	Case 1	61.2	59.4	54.9	83.1
	Case 2	20.8	46.3	30.4	42.7

Table 8 Average NMHC concentration (ppb) in the third and fifth model levels between 08:00 and 15:00 JST on August 6

Layer	Case	Nerima	Ebina	Saitama	Abiko
Layer 3	Case 1	179.9	108.5	147.3	114.5
	Case 2	125.9	39.5	89.4	69.6
Layer 5	Case 1	164.2	105.9	144.3	112.5
	Case 2	106.7	36.8	86.4	64.2

2.3 Influence of meteorological conditions on ozone simulations

The more accurate CMAQ simulation using Case 1 initial and boundary conditions was used to analyze the influence of meteorological conditions on ozone concentrations. Changes in local meteorological conditions such as solar radiation, wind direction, wind speed, relative humidity and temperature can greatly affect variations in ozone concentrations. Because the study periods analyzed here include only sunny days, our meteorological analyses focused on differences in wind, temperature and humidity between the two periods. Figure 7a shows the spatial distribution of the 2-m temperature and the 10-m winds from MM5 in the 3-km domain at 12:00 JST on July 22 and on August 6. July 22 was characterized by low temperatures and strong winds, with most of the Kanto area dominated by easterly and northeasterly winds. On August 6, the Tokyo Plain region had temperatures higher than 35°C and weaker southerly winds. Figure 7b shows the spatial distribution of relative humidity in the lowest level of the MM5 model, with July 22 generally more humid than August 6.

Figure 7c shows the spatial distribution of hourly-averaged predicted O_3 concentrations in the lowest CMAQ

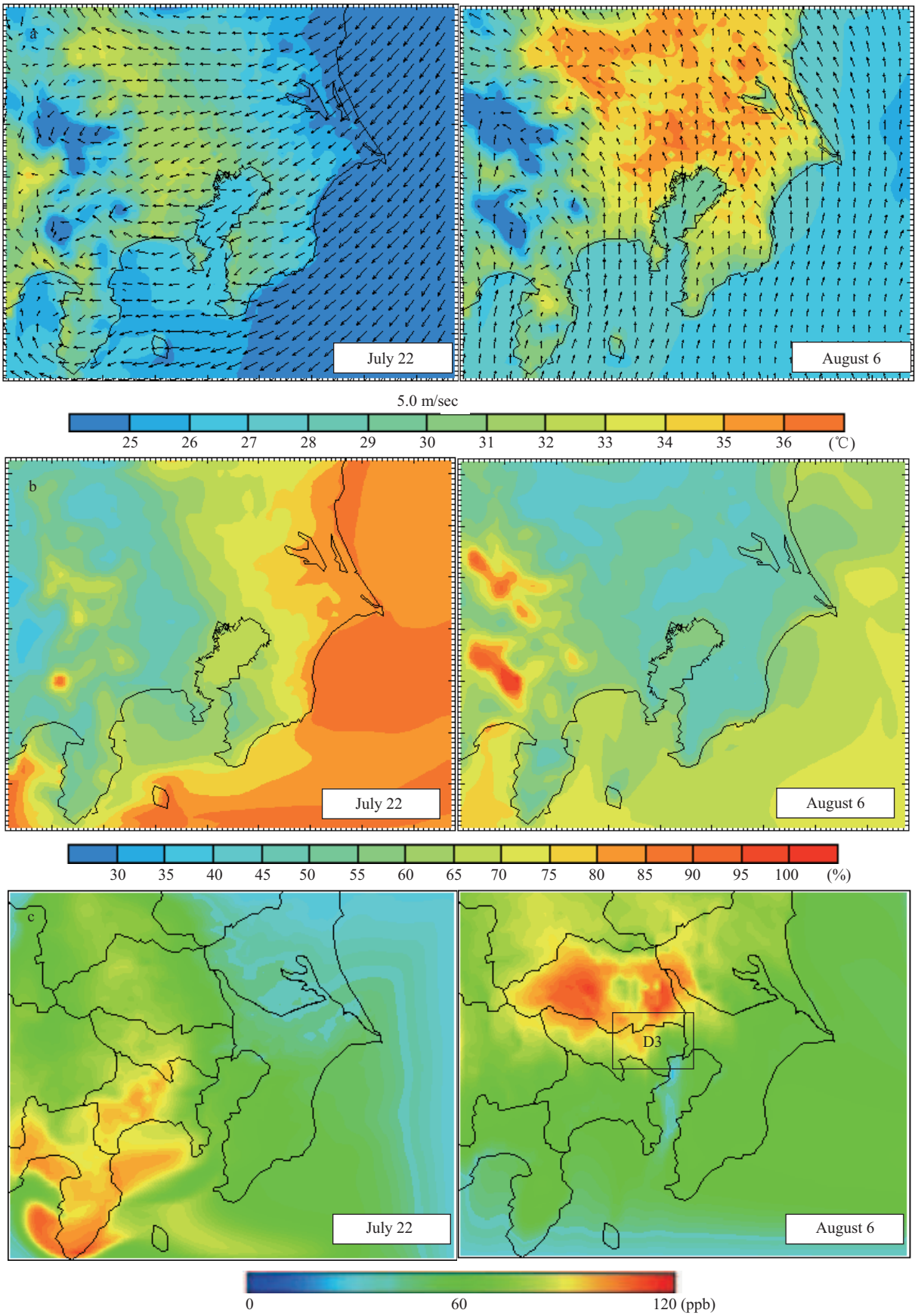

Fig. 7 MM5 simulated 2-m temperature & 10-m wind (a), MM5-simulated relative humidity (%) at the lowest model level (b), and CMAQ-simulated O_3 concentration (ppb) at the lowest model level (c) in Domain 2 at 12:00 JST for (a), (b), and 14:00 JST for (c).

model level (about 14 m) at 14:00 JST on July 22 and August 6. There are clear differences between the two days in the simulated spatial distribution and the location and magnitude of the predicted ozone maxima. As expected,

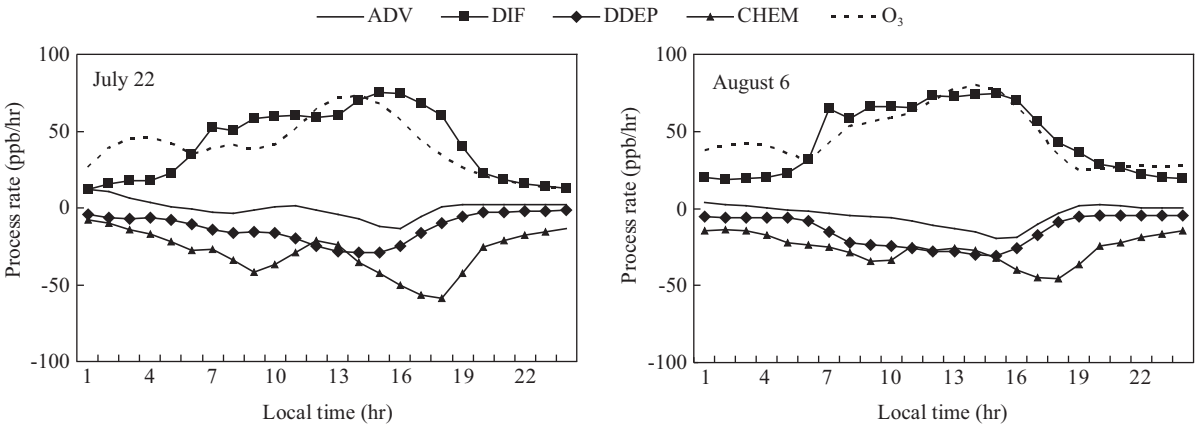

Fig. 8 Diurnal variation of the ozone rate of change in the first model level over the central Kanto area due to different processes on July 22 (a) and August 6 (b).

the ozone concentration is higher on the hot and dry day (August 6) than during the more mild conditions (July 22). High O_3 concentrations are also found in a larger region on August 6. On July 22, the northeasterly winds lead to southwestward transport of both ozone and primary pollutants emitted from the large coastal industrial zones around Tokyo Bay. Photochemical reaction of these pollutants leads to high ozone concentrations (> 90 ppb) in the southwestern part of Kanto. It should be noted that higher humidity over the northeastern seas on July 22 (> 85%) also has a significant effect on O_3 concentrations. Air masses transported from such moist sea areas are associated with lower temperatures, a condition that is not favorable for photochemical reactions. This may be one reason why the ozone concentration over central Kanto is lower on July 22 than on hotter days, which are often associated with dry air flow from the southern seas. In contrast to the July case, the hot and dry meteorological conditions on August 6 are conducive to photochemical O_3 production. The conditions on August 6 are typical of weather patterns generally associated with serious pollution in the Kanto metropolitan area. In our simulation, an area of high O_3 concentration covers most of the northwestern part of Kanto due to a transition from southward to southeasterward low predicted by MM5. As a result, some northern cities, including Saitama, Gunma, and Tochigi – have very high O_3 concentrations, while the southern part of Kanto is relatively free of ozone. The ozone maximum on this day reached 120 ppb in Saitama. These results are consistent with previous observational studies that found a strong relationship between atmospheric and surface transport mechanisms and the ozone distribution in the Kanto area (Wakamatsu et al, 1983; Uno et al, 1984).

We assessed the contributions of individual physical and chemical processes to ozone concentrations during the two meteorological conditions (Fig. 7c). Figure 8 summarizes the results of the process analysis for the central Kanto area on July 22 and August 6. The relative contributions of DIF and DDEP are higher than those of the other processes in both cases, although the different weather conditions lead to some differences. Table 9 shows that the deposition, diffusion, and advection terms are larger on August 6 than on July 22. In the first CMAQ model level, the advection-drive ozone transport out of the central Kanto area from 08:00 to 15:00 JST was –28.0 ppb on July 22 and –83.7 ppb on August 6. Some ozone may have been transported to the southwestern part of the area in July and to the northwestern part in August, contributing to the elevated ozone concentration in those regions. Meanwhile, there was less chemical ozone destruction (CHEM) on August 6 than on July 22. Meteorological conditions on August 6 were more favorable for photochemical ozone production, leading to a significant decrease in the net chemical consumption of ozone relative to July 22. Of the four main processes analyzed here, advection and diffusion showed the biggest differences between the two periods. We therefore conclude that the wind-driven transport of ozone and its precursors is the most important meteorological determinant of ozone concentration over the central Kanto area.

Table 9 Summary of the total change in ozone concentration (ppb/8 hr) due to different processes in the first model level during 08:00–15:00 JST

Episode	Process (ppb/8 hr)			
	ADV	CHEM	DIF	DDEP
July 22	–28.0	–265.2	493.2	–179.4
August 6	–83.7	–232.6	549.9	–212.5

3 Conclusions

In this article, we presented an evaluation of a numerical simulation of ozone over the Kanto area. We also analyzed the effects of the chemical initial and boundary conditions and meteorological conditions on the ozone simulations. Our results show that the coupled MM5/CMAQ model is a useful tool for the analysis of urban environmental issues. The simulation accurately reproduced most of the important characteristics of observational data from the Kanto region.

The initial and boundary conditions used in the model have a significant impact on simulated O_3 concentration. On hot and dry days with high O_3 concentration, the CMAQ model provides a poor simulation of peak O_3 concentrations when using the CMAQ default initial and boundary conditions, probably due to a significant decrease in photochemical ozone production associated with

low NMHC concentrations. The simulated O_3 concentrations are improved with the JCAP initial and boundary conditions (JCAP, 1999). On mild days, the CMAQ default initial and boundary conditions provide a more accurate simulation than the JCAP values.

We also find that terrestrial O_3 concentrations are strongly influenced by meteorological conditions over the Kanto area. Low O_3 concentrations are characteristic of mild weather conditions, while high concentrations are simulated during hot and dry conditions. The atmospheric and surface transport mechanisms have a significant effect on ozone distribution in the Kanto area. By investigating the effect of each process under different meteorological conditions, we found that advection and diffusion differed the most between the two periods. We therefore suggest that differences in wind speed and direction, which determine the transport of ozone and its precursors, might be the most important meteorological determinants of ozone concentration over the central Kanto area. However, accurately assessing the roles of different processes is a difficult problem due to the complex relationships between these processes. Therefore, better understanding of ozone formation necessitates a detailed analysis of the effects of physical and chemical processes on ozone concentrations during different weather conditions. We plan to address this issue in a subsequent investigation.

References

Berge E, Huang H C, Chang J, Liu T H, 2001. A study of the importance of initial conditions for photochemical oxidant modeling. *Journal of Geophysical Research*, 106(D1): 1346–1363.

Byun D, Ching J, 1999. Science algorithms of the EPA Models-3 Community Multiscale Air Quality (CMAQ) modeling system. US Environmental Protection Agency, EPA-600/R-99/030.

Chen D S, Cheng S Y, Liu L, Chen T, Guo X R, 2007. An integrated MM5-CMAQ modeling approach for assessing trans-boundary PM_{10} contribution to the host city of 2008 Olympic Summer Games – Beijing, China. *Atmospheric Environment*, 41: 1237–1250.

Dudhia J, 1989. Numerical study of convection observed during the winter monsoon experiment using a mesoscale two-dimensional model. *Journal of Atmospheric Science*, 46: 3077–3107.

Dudhia J, Gill D, Yong R G, Manning K, 2005. PSU/NCAR Mesoscale Modeling System. Tutorial Class Notes and User's Guide: MM5 Modeling System Version 3.

Grell G A, Dudhia J, Stauffer D R, 1994. A description of the fifth-generation Penn State/NCAR mesoscale model (MM5). NCAR Technical Note NCAR/TN-398+STR. 117.

US EPA (US Environmental Protection Agency), 2006. Guidance on the use of models and other analyses for demonstrating attainment of air quality goals for ozone, PM2.5, and regional haze, Draft 3.2, September 2006, http://www.epa.gov/scram001/guidance/guide/draft_final-pm-O3-RH.pdf.

Hayami H, Kobayashi S, 2004. Modeling of concentration of atmospheric secondary aerosol, CRIEPI Report T03037, 17.

Hong S Y, Pan H L, 1996. Nonlocal boundary layer vertical diffusion in a medium-range forecast model. *Monthly Weather Review*, 124: 2322–2339.

Hsie E Y, Anthes R A, 1984. Simulations of frontogenesis in a moist atmosphere using alternative parameterizations of condensation and precipitation. *Journal of Atmospheric Science*, 41: 2701–2716.

JCAP, 1999, Air Modeling (4), Observation results of Kanto area in summer, Technical Report of Japan Clean Air Program.

Jimenez P, Parra R, Baldasano J M, 2007. Influence of initial and boundary conditions for ozone modeling in very complex terrains: A case study in the northeastern Iberian Peninsula. *Environmental Modelling and Software*, 22(9): 1294–1306.

Kannari A, 2006. An analysis of weekend effects on photochemical oxidant concentrations in the Kanto and Kansai regions: Part 2 Verification of dynamically changing ozone formation regimes. *Journal of Japan Society for Atmospheric Environment*, 41(4): 220–233.

Kimura F, 1985. A numerical simulation of local winds and photochemical air pollution (II): Application to the Kanto Plain. *Journal of the Meteorological Society of Japan*, 63: 923–936.

Lamb R G, 1983a. A regional scale (1000 km) model of photochemical air pollution, Part I: theoretical formulation. EPA 600/3-83-035. U.S. Environmental Protection Agency, Research Triangle Park, NC.

Lamb R G, 1983b. A regional scale (1000 km) model of photochemical air pollution, Part II: input processor network design. EPA 600/3-84-085. U.S. Environmental Protection Agency, Research Triangle Park, NC.

Lippmann M, 1991. Health effects of tropospheric ozone. *Environmental Science and Technology*, 25: 1954–1962.

Liu T H, Jeng F T, Huang H C, Berge E, Chang J S, 2001. Influences of initial and boundary conditions on regional and urban scale Eulerian air quality transport model simulations. *Chemosphere Global Change Science*, 3: 175–183.

Morris R E, Meyers T C, 1990. User's guide for the Urban Airshed Model. In: User's manual for UAM(CB-IV). EPA-450/4-90-007A, vol. 1. U.S. Environmental Protection Agency Research Triangle Park, NC.

Ohara T, Wakamatsu S, Uno I, Ando T, Izumikawa S, Kannari A et al., 1997. Development and validation of numerical model for photochemical oxidants. *Journal of Japan Society for Atmospheric Environment*, 32(1): 6–28.

Sokhi R S, Jose R S, Kitwiroom N, Fragkou E, Perez J L, Middleton D R, 2006. Prediction of ozone levels in London using the MM5-CMAQ modeling system. *Environmental Modeling and Software*, 21: 566–576.

Uno I, Wakamatsu S, Ogawa Y, Murano K, 1984. Three-dimensional behaviour of photochemical pollutants covering the Tokyo metropolitan area. *Atmospheric Environment*, 18(4): 751–761.

Uno I, Ohara T, Sugata S, Kurokawa J, Furuhashi N, Yamaji K et al., 2005. Development of the RAMS/CMAQ Asian scale chemical transport modeling system. *Journal of Japan Society for Atmospheric Environment*, 40(4): 148–164.

Wakamatsu S, Ogawa Y, Murano K, Goi K, Aburamoto Y, 1983. Aircraft survey of the secondary photochemical pollutants covering the Tokyo metropolitan area. *Atmospheric Environment*, 17(4): 827–835.

Zhang Y, Liu P, Pun B, Seigneur C, 2006. A comprehensive performance evaluation of MM5-CMAQ for the summer 1999 southern oxidants study episode – Part I: Evaluation protocols, databases, and meteorological predictions. *Atmospheric Environment*, 40: 4825–4838.